Available online at www.sciencedirect.com
ScienceDirect
Journal of Power Sources 164 (2007) 631–638
JOURNAL OF POWER SOURCES
www.elsevier.com/locate/jpowsour

Lattice Boltzmann modeling of 2D gas transport in a solid oxide fuel cell anode

Abhijit S. Joshi, Kyle N. Grew, Aldo A. Peracchio, Wilson K.S. Chiu *

Department of Mechanical Engineering, University of Connecticut, 191 Auditorium Road, Storrs, CT 06269-3139, United States

Received 19 July 2006; received in revised form 27 October 2006; accepted 27 October 2006
Available online 6 December 2006

Abstract

Modeling of multi-component gas transport (H_2, N_2, H_2O) in a solid oxide fuel cell (SOFC) anode has been carried out using a recently developed two-dimensional (2D) lattice Boltzmann method (LBM) model. The LBM can simulate gas diffusion in complex porous media between species having different molecular weights. The porous anode structure through which gas transport occurs is obtained from micrograph images of an existing SOFC, converted to digital form and used as an input for the LBM model. Effect of medium geometry, mainly the porosity, and dimensionless flux on the fuel (H_2) delivery to the active sites and product (H_2O) removal is examined. The relationship between mass transfer and concentration polarization in the anode has been clarified. Predicted concentration polarization plots using the LBM model are validated against prior studies and show good agreement. Because of its ability to incorporate detailed geometry information, the LBM model can be used for design and optimization of SOFC electrodes without empirical modification of diffusion coefficients using medium porosity and tortuosity. As more advanced three-dimensional anode imaging techniques are developed, the LBM model can be adapted to model current flow through the anode material in addition to mass transport through the anode pores.

Keywords: Lattice Boltzmann method; SOFC; Concentration polarization; Anode microstructure; Multi-component diffusion; Porous media

1. Introduction

In a typical solid oxide fuel cell (SOFC) [Fig. 1(a)], an electrochemical reaction described by Eq. (1) occurs at the anode triple phase boundary (TPB). The anode TPB is the interface between the porous anode material (nickel yttria-stabilized zirconia, Ni + YSZ), electrolyte (YSZ) and the gas species (H_2 and H_2O) present in the pores. A hydrogen (H_2) molecule diffusing through the pores in the anode from the fuel or gas side at $x = 0$ to the TPB at $x = L$ combines with a negatively charged oxygen ion (O^{2-}) traveling through the solid electrolyte from the cathode side. H_2 forms a molecule of H_2O during this oxidation reaction and releases a pair of electrons

$$H_2 + O^{2-} \rightarrow H_2O + 2e^- \quad (1)$$

$$1/2O_2 + 2e^- \rightarrow O^{2-} \quad (2)$$

The H_2O molecule formed at the TPB then diffuses back through the pores in the anode from $x = L$ towards the gas channel at $x = 0$. The electrons generated at the anode TPB are conducted through the anode material to the current collector, and flow through an external circuit. The electrons finally enter the cathode and are conducted through the cathode material to the cathode TPB. Here, the electrons combine with oxygen that has diffused from the air through pores in the cathode to create O^{2-} ions as indicated in Eq. (2). These ions are conducted through the electrolyte and the cycle is completed. Assuming that each hydrogen molecule is consumed and forms a water molecule at the anode TPB, the mole flux of hydrogen is equal and opposite to the mole flux of water vapor. This case is often referred to as equimolar counter-diffusion. Actual diffusion in the porous anode occurs in the presence of a third species, nitrogen (N_2). The N_2 takes no active part in the chemical reaction; however the presence of N_2 affects transport of other species within the fuel cell.

The goal of this work is to model the diffusive flow of three species (H_2, H_2O and N_2) through the porous anode structure using a two-dimensional (2D) representation, so that transport

* Corresponding author. Tel.: +1 860 486 3647; fax: +1 860 486 5088.
E-mail address: wchiu@engr.uconn.edu (W.K.S. Chiu).

0378-7753/$ – see front matter © 2006 Elsevier B.V. All rights reserved.
doi:10.1016/j.jpowsour.2006.10.101

Nomenclature

C_T	total molar concentration (mol m^{-3})
D_{12}	binary diffusivity between H_2 and H_2O (m^2 s^{-1})
D_{23}	binary diffusivity between H_2O and N_2 (m^2 s^{-1})
D_{31}	binary diffusivity between N_2 and H_2 (m^2 s^{-1})
e	base velocity in the lattice Boltzmann model
E	actual voltage developed by the fuel cell (V)
E_0	maximum voltage (V)
f	particle velocity distribution function
F	Faradays constant (96,485 A s mol^{-1})
H	height of the model anode (m)
i	current density (A m^{-2})
i^*	non-dimensional current density
J	mole flux (mol m^{-2} s^{-1})
J^*	dimensionless flux = JL/C_TD_{23}
L	total thickness of the anode (m)
N	number of processors used in a parallel computation
P	partial pressure
R	universal gas constant (8.3145 J mol^{-1} K^{-1})
t	time (s)
x	distance in the anode, measured from the gas side (m)
x	position of a lattice node
x^*	distance normalized by the total length
X	mole fraction
z	distance measured parallel to anode surface in the gas channel (m)

Greek letters

α	lattice direction
ϕ	porosity
Ω	collision term

processes can be better understood and thus optimized with respect to the porous geometry, leading to improvements in SOFC performance. A detailed understanding of mass transfer is one of the first steps in developing a comprehensive mathematical model of a SOFC. Additional effects including surface adsorption/desorption and chemical reactions (important for simulating internal reforming), while important, are beyond the scope of this article. The two-dimensional model of the porous SOFC anode is shown in Fig. 1(b). The mole fractions of H_2, H_2O and N_2 are known at the fuel or gas side and the mole flux of H_2 (and hence of H_2O) is known at the TPB based on the current drawn by the SOFC. For simplicity, the TPB is treated like an infinitely thin boundary in this study, although the model developed here can easily be adapted for the case where the exact geometric location of the TPB is available from imaging techniques. The solid obstacles are impermeable to all species and no-slip boundary conditions are applied at the obstacle surfaces. Along the z direction, a reasonable height H is used so that it allows a realistic representation of the porous geometry. Periodic boundary conditions are employed at $z = 0$ and $z = H$ for

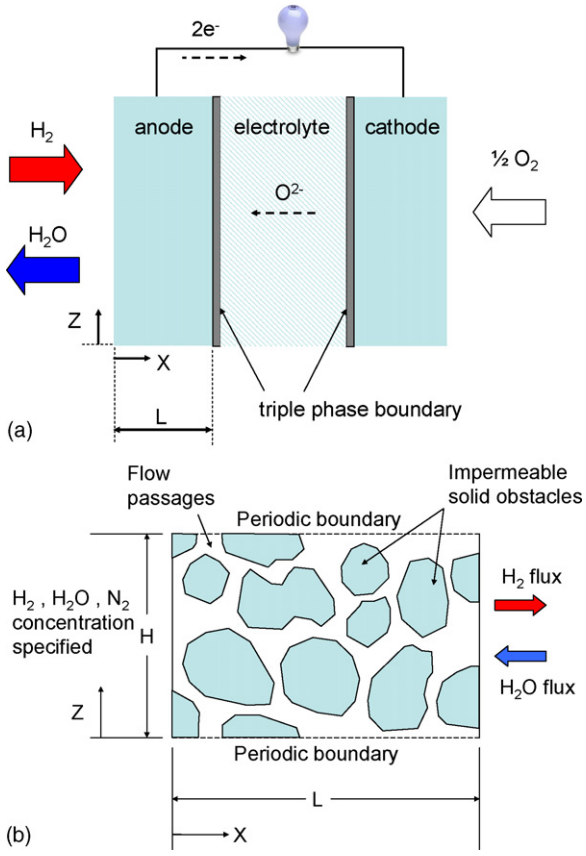

Fig. 1. (a) Solid oxide fuel cell. (b) Model of the porous anode.

computational efficiency. Because the intended application is an anode supported SOFC, diffusion of O_2 through the cathode is not modeled.

The lattice Boltzmann method (LBM) is used to model species transport through the porous anode. In recent times, the LBM has been well established as an alternative computational fluid dynamics (CFD) approach for a variety of applications [1]. The LBM has been gaining popularity owing to its ease of implementation and ability to capture the right physics of flow and diffusion over a wide range of Knudsen numbers compared to the more traditional approaches based on the Navier–Stokes equations. Of the many LBM variants designed to model multi-component diffusion, the method chosen here is based on the two-fluid model initially proposed by Luo and Girimaji [2] and extended by McCracken and Abraham [3] in order to model components with different molecular weights. It has been shown that LBM can model single-component flow in the non-continuum flow regime [4,5]. This feature is important for SOFC applications because high temperatures and small pore sizes cause non-continuum diffusion effects to become important. However, capability of the LBM to model non-continuum mass diffusion is the focus of a separate study within our group and this work focuses on continuum transport. The LBM is developed for three gaseous species (1 = H_2, 2 = H_2O, 3 = N_2) with no phase changes. It is assumed that the mass diffusion occurs at constant temperature and transport properties like binary diffusion coefficients are constant. The LBM model used here has

been validated with the Stefan–Maxwell (SM) equations for simplified geometries in both 1D and 2D cases [6].

Modeling of mass transport in a SOFC has been performed by a large number of research groups, [7–15]. However, in most of these prior studies, parameters such as the porosity, tortuosity, and mean pore radius influence mass transport through the porous medium and affect eventual predictions of cell performance. While the porosity and mean pore radius can be measured experimentally, tortuosity is often obtained via empirical relations that can change from one microstructure to the next. Thus, these models do not have the capability to model the fundamental effects of electrode geometry on SOFC mass transport. The goal of the present work is to use the LBM approach to model multi-component diffusion in complex geometries without relying on empirical factors like tortuosity. The relationship between mass transport and concentration polarization is directly explored for geometries representative of actual SOFC anodes.

The remaining part of the paper is organized as follows. In Section 2, the LBM for three-component diffusion used in the present study is reviewed. Parallel implementation of the LBM algorithm is discussed next with the help of speed up plots. Imaging techniques used to obtain a digital representation of the anode geometry are described in Section 3. Results obtained from the LBM model, parametric studies and validation of LBM model results are discussed in Section 4 and conclusions are presented in Section 5.

2. Lattice Boltzmann method

The first step in the LBM is to overlay the solution domain with a discrete lattice consisting of a network of node points. A uniform, square lattice is used, with obstacles occupying part of the lattice. The LBM essentially consists of two basic steps that are carried out at each node point **x** that is not inside an obstacle: streaming and collision. Streaming represents movement of particles of each species i (where $i = 1$, 2 or 3) along specified, nearest neighbor lattice directions $\mathbf{e}_\alpha^i$ $\{\alpha = 0, 1, 2, 3, 4, 5, 6, 7, 8\}$. These velocity directions are based on the D2Q9 model [16]. The collision term represents interactions between particles of the same or different species as they arrive at any given node. These steps are combined together in Eq. (3), which is called as the lattice Boltzmann equation.

$$f_\alpha^i(\mathbf{x} + \mathbf{e}_\alpha^i, t + 1) - f_\alpha^i(\mathbf{x}, t) = \Omega_\alpha^i \tag{3}$$

In Eq. (3), f_α^i is the velocity particle distribution function (PDF) along direction $\mathbf{e}_\alpha^i$, t is the time-level and Ω_α^i represents the collision term for species i along the direction α. Physically, f_α^i at any given location **x** represents the number of particles of species i at that location likely to be moving with a velocity of $\mathbf{e}_\alpha^i$. Eq. (3) essentially provides a time marching scheme to advance the PDFs in time at each lattice point. Moments of the PDF f_α^i over velocity space lead to the species density and velocity.

Boundary conditions on the PDF at the left and right boundary of the solution domain illustrated in Fig. 1(b) are assigned based on a treatment similar to that used by Zou and He [17], but are modified such that the average velocity before and after collision is used [18]. Particle density (mole fraction) is specified at $x = 0$ and the x-component of particle velocity (mole flux) is specified at $x = L$ for H_2 and H_2O. For the inert N_2, the mole flux at the TPB is zero. Obstacles within the domain are treated like impermeable solids with zero mass flux in a direction normal to their surface. The tangential velocity of all species at solid obstacles is also assumed to be zero. To implement these conditions in the LBM model, bounce-back conditions [17] are used on lattice points corresponding to obstacles. Species mole fractions are initially assigned the same values over the entire domain and these are their respective values at $x = 0$. The x-component of species velocities (for H_2 and H_2O) are initially based on the inlet concentration and specified mole flux at $x = L$. The y-component of velocity is initially zero everywhere in the solution domain. For lattice points that lie on the solid boundary, both velocity components are zero. Using Eq. (3), the PDFs are then evolved in time until a steady solution is obtained.

The LBM algorithm used in this work [6] is implemented in parallel on a SGI Altix 3700 at the University of Connecticut. A vertical decomposition of the solution domain is carried out with each processor handling a specific number of rows. Fig. 2(a) shows an example anode geometry modeled using a 51×51 lattice, with calculations split among five processors. The message passing interface (MPI) library is used for communication of data between processors during each time step. In the input geometry file shown in Fig. 2(a), solid obstacles are represented by 0 and gas flow passages are represented by 1. This input file is created using image processing techniques discussed in Section 3.

For a parallel simulation, speed-up for N processors is defined as the ratio of run-time for a single processor to the run-time using N processors. Ideally, if N processors are used, the run-time should fall by a factor of N, leading to a speed-up of N. A speed up plot for typical LBM model runs is shown in Fig. 2(b). The white bars indicate the ideal or linear speed-up. It can be seen that the actual speed-up (indicated by the colored bars) falls short of linear, especially for large N. This occurs due to the relatively large time spent in communicating data between processors. However, a reasonable speed-up is obtained, allowing for cases studied to achieve convergence in a reasonable time. It is also quite encouraging that for large grid sizes, the LBM exhibits linear speed up through a larger number of processors. The current LBM code is thus readily portable onto larger vector computers for solving more complex problems using a higher lattice resolution.

3. Imaging anode microstructure

At present, SEM images like the one shown in Fig. 3 are first used to construct a detailed model image. This image (black and white) is similar to the microstructure image, but has a better contrast between solid and void spaces. The model image is then converted to a digital format where solid (black) and void (white) regions are represented by 0 and 1, respectively. The conversion is performed using ImageJ (http://rsb.info.nih.gov/ij/). In reality, the pores are connected via pathways in and out of

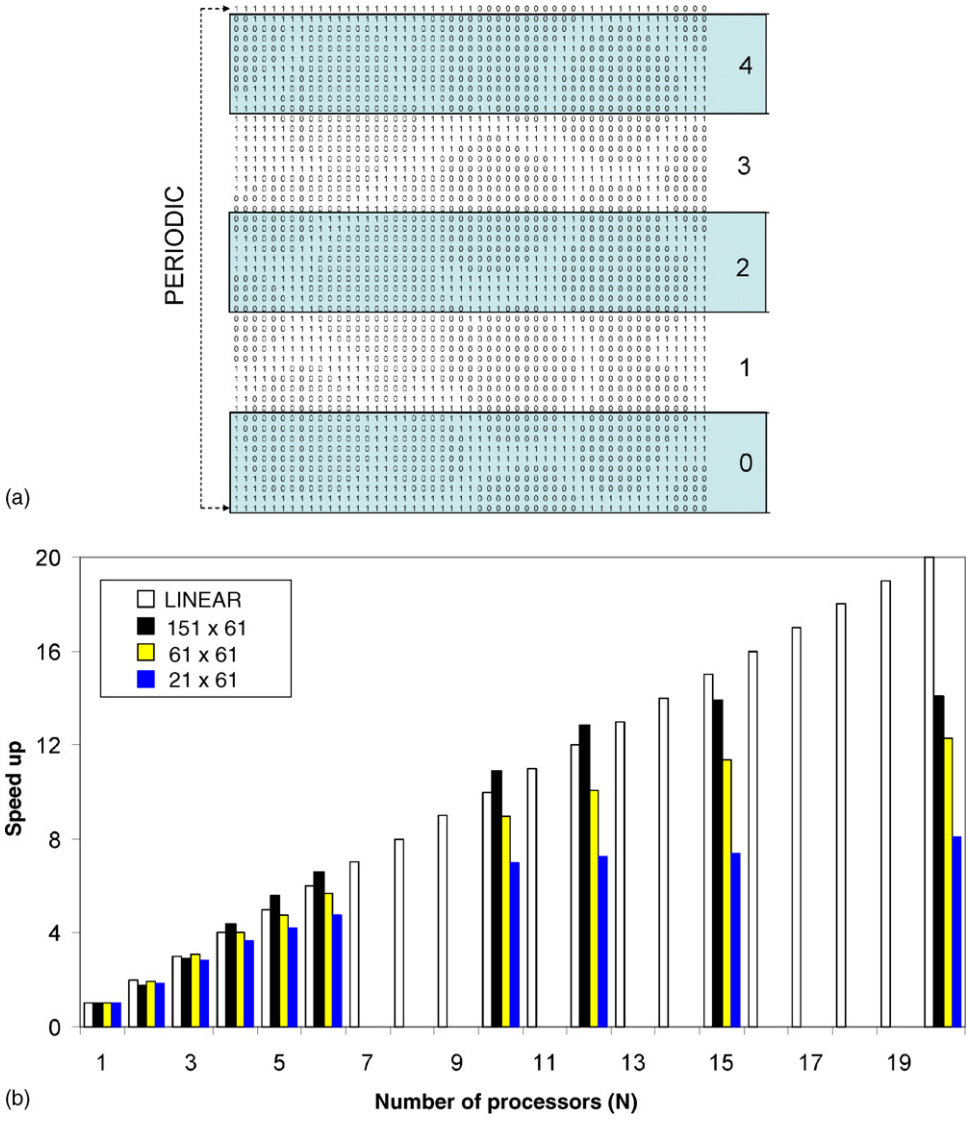

Fig. 2. (a) Vertical decomposition of a 51 × 51 lattice using five processors. (b) Speed up behavior of the LBM model using vertical decomposition.

the plane of the image, but this information can not be obtained without using a 3D imaging technique. Thus, while constructing the model image, it is sometimes necessary to artificially change the digitized image to provide a connected network of pores and thus have clear pathways for mass diffusion. In addition to the above limitation, the anode materials used for SEM (obtained from actual SOFC prototypes) are of a fixed porosity value (∼30%) and geometry data for different porosities is not available. In order to carry out parametric studies, the porosity is reduced by enlarging the size of solid obstacles (reducing void spaces) and by adding more obstacles in the domain if necessary. Because of these limitations, the 2D geometry should be viewed as qualitatively resembling actual SOFC anodes. A more accurate representation will have to wait until more advanced 3D imaging techniques are available. The lattice size for the LBM will need to be large enough to adequately resolve the microstructure. At the same time, it should lead to reasonable run-times. Run time for a 151 × 151 lattice using 25 processors was about 135 min.

4. Results and discussion

The two main dimensionless parameters governing continuum mass transport through a porous medium are the porosity ϕ, which is defined as the fraction of anode area (volume in 3D) occupied by void space, and the dimensionless flux (J^*)

$$J^* = \frac{JL}{C_T D_{31}} \tag{4}$$

In Eq. (4), J is the mole flux at the TPB, L is the length of the medium, C_T is the total molar concentration, and D_{31} is the binary diffusion coefficient between H_2 and N_2. Physically, J^* represents the relative strength of convective and diffusive mass transport of hydrogen gas through N_2. Because mass transport in a SOFC tends to be diffusion dominated, values of J^* tend to be quite small, typically of the order of 10^{-2}. LBM parameters can be arbitrarily chosen as long as the corresponding dimensionless numbers are correct. For example, to simulate a case where $J^* = 0.16$, the LBM parameters (in lattice units) can be: $L = 150$,

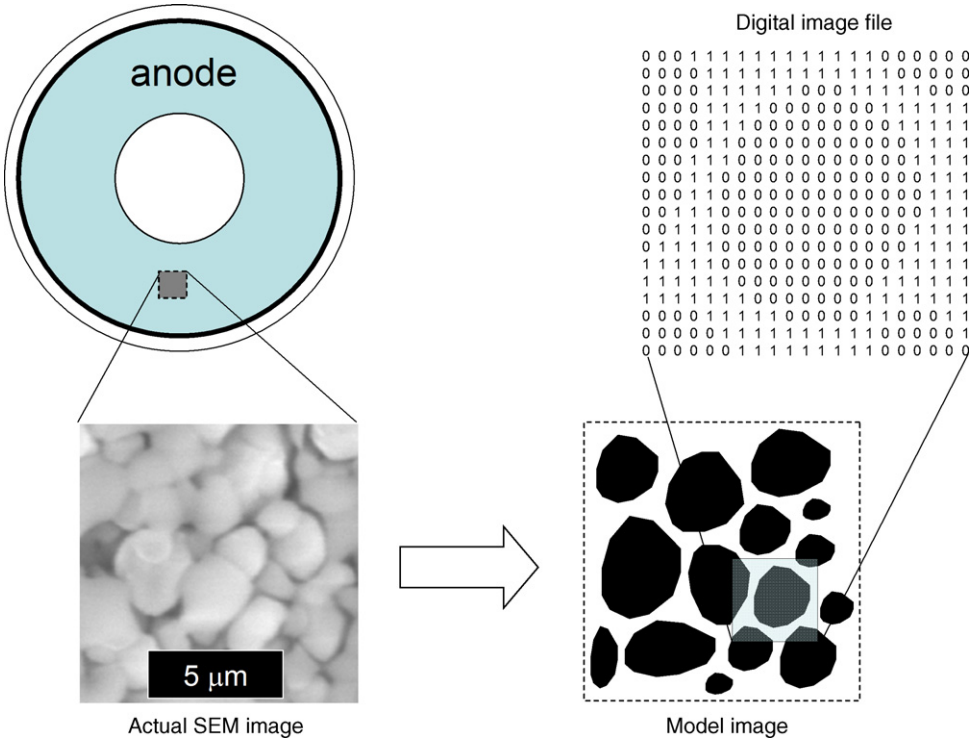

Fig. 3. Construction of digital geometry input file from a SEM image.

$J = 0.069$, $C_T = 600$, $D_{12} = 0.337$, $D_{23} = 0.069$ and $D_{31} = 0.1085$. Unless indicated otherwise, mole fractions of H_2, H_2O and N_2 are 0.47, 0.03 and 0.5, respectively at $x = 0$. Because it involves the mole flux, J^* can be related to the current density of the fuel cell via [19]

$$i = 2F \times J \tag{5}$$

In Eq. (5), i is the current density and F is Faraday's constant. In the present study, the mole flux remains constant over the TPB, leading to a constant current density at the anode–electrolyte interface. The current is non-dimensionalized using $i^* = iL/(2FC_TD_{31}) = J^*$. The voltage or EMF developed by the cell E can be obtained using the fuel (H_2), product (H_2O) and oxygen (O_2) partial pressures (or mole fractions) at the TPB in the Nernst equation [19]

$$E = E^0 + \frac{RT}{2F} \ln \left[\frac{P_{H_2} P_{O_2}^{0.5}}{P_{H_2O}} \right] \tag{6}$$

In Eq. (6), E^0 is the EMF at standard pressure and R is the gas constant. As mentioned, diffusion through the cathode is not modeled and the partial pressure of O_2 at the cathode TPB is assumed to be a constant 21%. The concentration polarization (ΔV_{conc}) is defined to be the loss of voltage due to the drop in fuel (H_2) concentration across the anode from the gas channel $x = 0$ to the TPB $x = L$.

$$\Delta V_{conc} = E_{gas\ channel} - E_{TPB} \tag{7}$$

In Eq. (7), $E_{gas\ channel}$ is evaluated using H_2 and H_2O mole fractions of 0.47 and 0.03 respectively, while E_{TPB} is evaluated based on the average H_2 and H_2O mole fractions obtained at $x = L$ from the LBM model.

4.1. Validation of the LBM model

Experimental data for just concentration polarization is scarce, so the LBM results have been compared with some prior models that calculate concentrcaation polarization (Chan et al. [8], Zhao and Virkar [10]). In order to have a fair comparison, the dimensional current i used in these prior models needs to be converted to a non-dimensional current density i^*. This conversion is illustrated for one particular case. The following data for the anode is obtained from Chan et al. [8]: porosity = 30%, tortuosity = 6, $L = 750 \times 10^{-6}$ m. Based on Eq. (5), a current density $i = 20{,}000\ A\ m^{-2}$ corresponds to a mole flux $J = 0.1036\ mol\ m^{-2}\ s^{-1}$. The binary diffusivity is $D_{13} = 1.085 \times 10^{-4}\ m^2\ s^{-1}$ and $C_T = 11.4\ mol\ m^{-3}$ at a pressure $P = 1$ atm and temperature $T = 1073$ K based on the ideal gas law. Note that tortuosity is not a parameter in the LBM model, but is an empirical parameter used to change the binary diffusivity value by Chan et al. [8], Zhao and Virkar [10] and by many other models that are based on a 1D representation of the porous medium. The above set of parameters $\{L, J, C_T, D_{13}\}$ lead to $J^* = i^* = 0.0628$. Thus, a current density $i = 20{,}000\ A\ m^{-2}$ in the study by Chan et al. [8] corresponds to a non-dimensional current density $i^* = 0.0628$. This relationship is used to convert the data provided by Chan et al. [8] (Fig. 3 from their paper) to dimensionless form. A similar conversion is performed on the data provided by Zhao and Virkar [10] in Fig. 21 of their paper. This latter study has a porosity of 32%, which is fairly close to the 30% porosity data calculated using the LBM model.

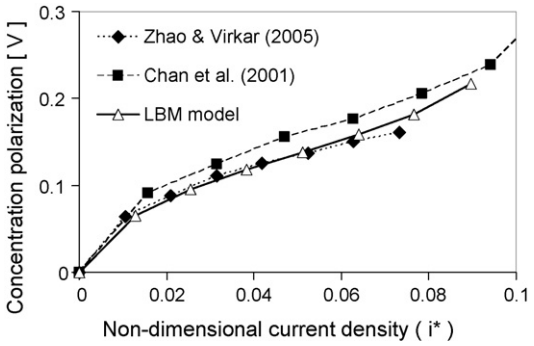

Fig. 4. Validation of the LBM model for a porosity of 30%.

Fig. 4 compares the concentration polarization from the LB model with data from Chan et al. [8] and Zhao and Virkar [10]. The LBM polarization curve corresponds to the 30% porosity data from Fig. 8, with many additional data points. It can be observed that Chan et al. [8] predict an initially convex and ultimately concave shape of the concentration polarization curve. However, the limiting current density in the LBM model is lower, so the entire portion of the concave part of the curve (for large i^*) is not obtained at 30% porosity. This concave region is also absent in the results of Zhao and Virkar [10]. It is observed the LBM model predictions are fairly close to these two prior models, indicating that the LBM approach is accurate enough to model concentration polarization in a SOFC using a 2D model.

The differences observed in the predicted concentration polarization may be because of the 2D geometry used in this work, non-continuum effects and/or because of empirical factors like tortuosity used in prior models. The electrochemical coupling between current density and species concentration may be important when the limiting current condition is reached. In addition, it should also be pointed out that the LBM model presented here uses a ternary system $\{H_2, H_2O, N_2\}$, while both Chan et al. [8] and Zhao and Virkar [10] employ a binary system of H_2 and H_2O.

4.2. Mass transport through porous media

Fig. 5 illustrates a typical, steady state, mole fraction variation of H_2, H_2O and N_2 inside the porous anode for $\phi = 0.5$ and $J^* = 0.16$. A high value of $J^* = 0.16$ is used in order to clearly indicate mole fraction variation of H_2, H_2O and N_2 in a typical porous geometry. Smaller values of J^* do not produce appreciable changes in species mole fractions. In general, diffusive mass transport of any species occurs from higher to lower concentrations. Because H_2 is consumed at the TPB, the mole fraction of H_2 at the TPB is lower compared to the gas side. Similarly, as H_2O is generated at the TPB, mole fraction of H_2O at the TPB is higher. For the inert N_2, even if there is no mass transfer, the mole fraction at the TPB reduces. For all three species, mole fraction at the TPB varies with z depending on the local structure of the porous medium. Therefore, mole fractions of H_2 and H_2O at the TPB are averaged along z for parametric studies and for calculating the concentration polarization.

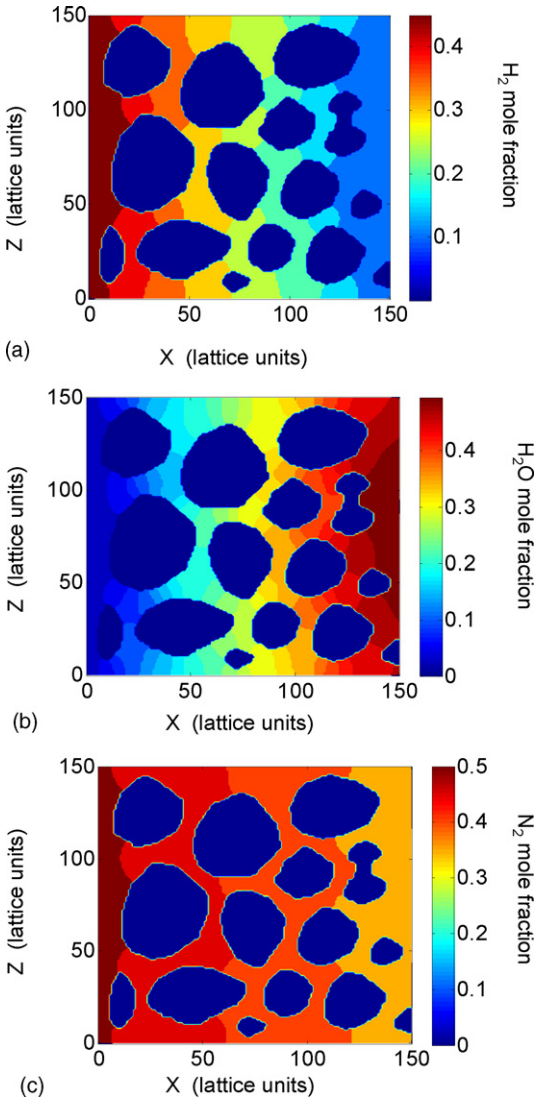

Fig. 5. Mole fraction distribution for H_2 (a), H_2O (b) and N_2 (c) inside a porous anode for $\phi = 0.5$ and $J^* = 0.16$.

4.3. Effect of porosity and dimensionless flux on mass transport

The porosity in the LB model is controlled by changing the amount of void spaces present in the solid matrix. Anodes of different porosities from $\phi = 0.25$–0.5, constructed using a 151×151 lattice, are shown in Fig. 6. For a given J^*, as the porosity reduces, there are less diffusion pathways through the domain and a larger concentration difference is required in order to maintain the same amount of molar flux. As the mole fraction of H_2 is fixed at $x = 0$, the mole fraction of H_2 at the TPB reduces as the porosity reduces. The mole fraction values at a porosity of 100% correspond to the case where there are no obstacles. As a check, it is verified that predicted values using the LB model match those obtained from the 1D solution to the SM equations. For a fixed porosity value, as J^* is increased, concentration gradient increases to accommodate the larger mole flux. Due to increased current draw, H_2 mole

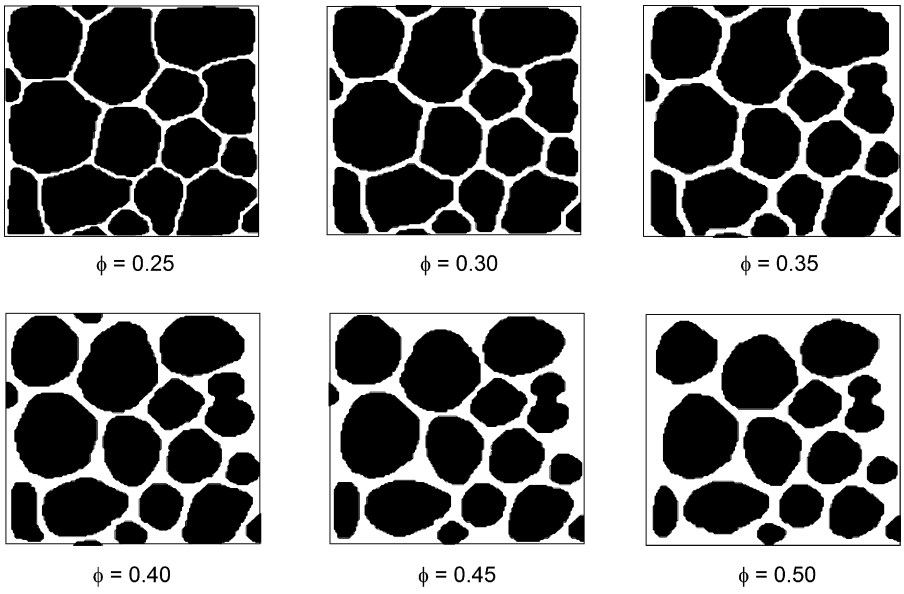

Fig. 6. Anode geometries used to study the effect of porosity (ϕ) with a 151 × 151 lattice.

fraction at the TPB reduces. If J^* is too large, the limiting current condition is reached because the H_2 concentration at the TPB tends to approach zero. This effect is magnified at low porosity values. Thus, a limit is imposed on the magnitude of J^*.

Both of these effects are illustrated in Fig. 7, which plots the average H_2 mole fraction at the TPB as a function of porosity for different J^* values. It can be seen that for high J^*, the porosity has to be above a threshold value for solutions to be obtained. The variation with porosity is highly non-linear, except for the trivial case of $J^* = 0$, representing no current draw. This study assumes that the current density at the TPB is independent of species concentration at that point. A detailed analysis is currently in progress in order to establish the nature of the interdependence of the diffusion and electrochemical reaction processes. Once this analysis is complete, the LBM model can be suitably adapted to take this coupling into account if required.

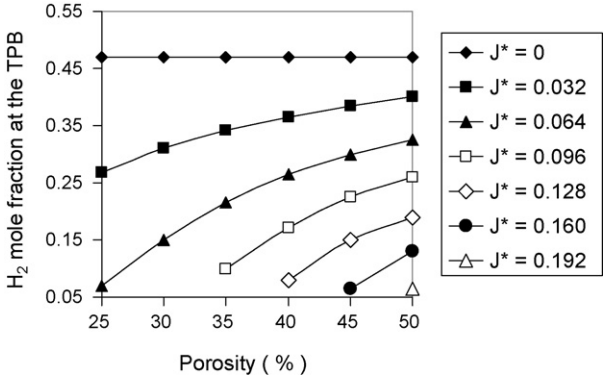

Fig. 7. Effect of porosity and J^* on H_2 mole fraction at the TPB. LBM parameters (in lattice units): $L = 150$, $J = 0.069$, $D_{12} = 0.337$, $D_{23} = 0.069$ and $D_{31} = 0.1085$. Mole fractions of H_2, H_2O and N_2 are 0.47, 0.03 and 0.5 respectively at $x = 0$. J^* changed by changing the value of C_T.

4.4. Effect of porosity and dimensionless flux on concentration polarization

Once the average H_2 and H_2O mole fractions at the anode TPB are known from the LBM, anode concentration polarization curves can be constructed using Eq. (7) to study SOFC performance. Because lower fuel concentration at the TPB leads to higher polarization losses, it can be deduced that these losses are more for low porosity values and high J^* (larger current density). Concentration polarization curves are calculated for a range of i^* values and for different anode porosities in Fig. 8. It is found that the polarization curve is almost linear at intermediate i^*, with steeper gradients at the lower and higher ends. As expected, since i^* is proportional to J^*, the lowest polarization occurs at small i^*.

The general trend of the polarization curve is similar for different anode porosities. However, for a given current density i^*, as the porosity is reduced, the polarization increases. This is due to the reduction in H_2 mole fraction at the anode TPB

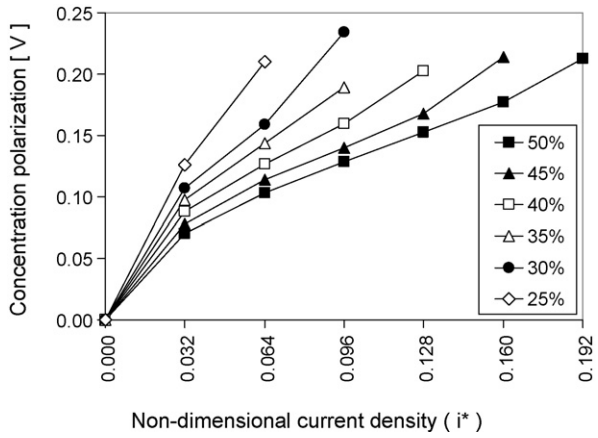

Fig. 8. Anode concentration polarization for different porosity values.

at low porosity. The maximum current drawn by the SOFC is also smaller for a low porosity. In Fig. 8, the increasing slopes of the polarization curves indicate that the polarization is more sensitive to changes in current density at low porosities. Some curves in Fig. 8 stop at a lower voltage because solutions are not obtained at the next i^* value due to the H_2 mole fraction becoming zero (limiting current condition).

Increasing the anode porosity leads to better mass transport of fuel and lower concentration polarization. However, a high porosity can reduce the number of electrochemical reaction sites as well as the pathways for the flow of electrons through the anode, thereby increasing activation and ohmic losses (not modeled here). High porosity can also lead to reduced mechanical strength. An optimum porosity and microstructure geometry may exist where the combined polarization losses (concentration + activation + ohmic) are a minimum. In practice, the porosity is often comparatively larger near the gas channel and is lower near the electrolyte to provide more surface area for electrochemical reactions to take place. Using the LBM model developed here, SOFC anode microstructure can be optimized to give the best performance.

5. Conclusions

The lattice Boltzmann method (LBM) is used as a tool to model mass transport of H_2 (fuel) and H_2O (product) in the presence of N_2 (inert gas) in the porous anode structure of a SOFC. The porous structure used in the LBM model is based on SEM images, which are converted to digital form. Results for mole fraction distributions are obtained for a range of porosity values and dimensionless flux values. For high porosity, predictions using the LB model approach those obtained from solving the continuum, 1D Stefan–Maxwell equations. As porosity is reduced, the fuel concentration at the TPB rapidly falls and eventually approaches zero. For any porosity, there is a condition of maximum J^* above which a limiting current density in the SOFC can be predicted.

Advantages of the LBM model are that a detailed analysis of mass transfer can be carried out for an actual anode microstructure and fuel cell performance can be judged by calculating the concentration polarization. Complex geometries can be easily handled and both continuum and non-continuum diffusion through the pores can be modeled. Because of the level of detail, effect of anode geometry on voltage polarization can be directly studied and the geometry optimized to give the best performance. Unlike prior models, empirical parameters like tortuosity are not used as fitting parameters to account for the porous medium.

A limitation of the present study is the absence of three-dimensional (3D) connectivity of the anode pore structures, but this will be overcome in the future as better image processing techniques start becoming available. Some recent image processing work [20] is a step in the right direction, but non-destructive imaging techniques like XMT that will minimize disruption of the anode microstructure also need to be developed further. The LBM model itself can be adapted to 3D and boundary conditions can be changed such that species generation and consumption can be applied at specific TPB locations within the microstructure. In addition to mass transport, activation and ohmic losses in the anode will be considered in future studies as 3D imaging data becomes available. Incorporation of these effects in the present LBM model will lead to a highly accurate and useful tool for SOFC design and analysis.

Acknowledgments

Financial support from the Army Research Office is gratefully acknowledged. SOFC anode samples were provided by Adaptive Materials Inc. (Ann Arbor, MI). We thank Francesco De Carlo (Advanced Photon Source, Argonne, IL) for valuable discussions on image processing using ImageJ.

References

[1] S. Chen, G.D. Doolen, Ann. Rev. Fluid Mech. 30 (1998) 329–364.
[2] L.S. Luo, S.S. Girimaji, Phys. Rev. E 67 (2003) 036302.
[3] M.E. McCracken, J. Abraham, Phys. Rev. E 71 (2005) 046704.
[4] G.H. Tang, W.Q. Tao, Y.L. He, Phys. Fluids 17 (2005) 058101.
[5] F. Toschi, S. Succi, Europhys. Lett. 69 (4) (2005) 549–555.
[6] A.S. Joshi, K.N. Grew, A.A. Peracchio, W.K.S. Chiu, Lattice Boltzmann method for continuum, multi-component diffusion in complex 2D geometries, J. Appl. Phys., submitted for publication.
[7] M.M. Hussain, X. Li, I. Dincer, Int. J. Energy Resour. 29 (2005) 1083–1101.
[8] S.H. Chan, K.A. Khor, Z.T. Xia, J. Power Sources 93 (2001) 130–140.
[9] S.H. Chan, Z.T. Xia, J. Electrochem. Soc. 148 (2001) A388–A394.
[10] F. Zhao, A.V. Virkar, J. Power Sources 141 (2005) 79–95.
[11] Z.T. Xia, S.H. Chan, K.A. Khor, Electrochem. Solid State Lett. 7 (3) (2004) A63–A65.
[12] H. Yakabe, M. Hishinuma, M. Uratani, Y. Matsuzaki, I. Yasuda, J. Power Sources 86 (2000) 423–431.
[13] P.W. Li, L. Schaefer, M.K. Chyu, ASME J. Heat Trans. 126 (2004) 219–229.
[14] E.S. Greene, W.K.S. Chiu, M.G. Medeiros, J. Power Sources 161 (2006) 225–231.
[15] W. Lehnert, J. Meusinger, F. Thom, J. Power Sources 87 (2000) 57–63.
[16] Y.H. Qian, D. D'Humieres, P. Lallemand, Phys. Rev. Lett. 56 (14) (1986) 1505–1508.
[17] Q. Zou, X. He, Phys. Fluids 9 (6) (1997) 1591–1598.
[18] X. Shan, G. Doolen, Phys. Rev. E 54 (4) (1996) 3614–3620.
[19] J. Larminie, A. Dicks, Fuel Cell Systems Explained, John Wiley and Sons, West Sussex, UK, 2003.
[20] J.R. Wilson, W. Kobsiriphat, R. Mendoza, H.Y. Chen, J.M. Hiller, D.J. Miller, K. Thornton, P.W. Voorhees, S.B. Adler, S.A. Barnett, Nat. Mater. 5 (2006) 541–546.